JACS
JOURNAL OF THE AMERICAN CHEMICAL SOCIETY
pubs.acs.org/JACS
Article

A Combined Computational and Experimental Study of Rh-Catalyzed C−H Silylation with Silacyclobutanes: Insights Leading to a More Efficient Catalyst System

Linxing Zhang,[#] Kun An,[#] Yi Wang,[#] Yun-Dong Wu, Xinhao Zhang,* Zhi-Xiang Yu,* and Wei He*

Cite This: J. Am. Chem. Soc. 2021, 143, 3571−3582

Read Online

ACCESS | Metrics & More | Article Recommendations | Supporting Information

ABSTRACT: The study of new C−H silylation reagents and reactions remains an important topic. We reported that under Rh catalysis, silacyclobutanes (SCBs) for the first time were able to react with C(sp^2)−H and C(sp^3)−H bonds, however the underlying reasons for such a new reactivity were not understood. Through this combined computational and experimental study on C−H silylation with SCBs, we not only depict a reaction pathway that fully accounts for the reactivity and all the experimental findings but also streamline a more efficient catalyst that significantly improves the reaction rates and yields. Our key findings include: (1) the active catalytic species is a [Rh]−H as opposed to the previously proposed [Rh]−Cl; (2) the [Rh]−H is generated via a reductive elimination/β-hydride (β-H) elimination sequence, as opposed to previously proposed endocyclic β-H elimination; (3) the regio- and enantio-determining steps are identified; (4) and of the same importance, the discretely synthesized [Rh]−H is shown to be a more efficient catalyst. This work suggests that the [Rh]−H/diphosphine system should find further applications in C−H silylations involving SCBs.

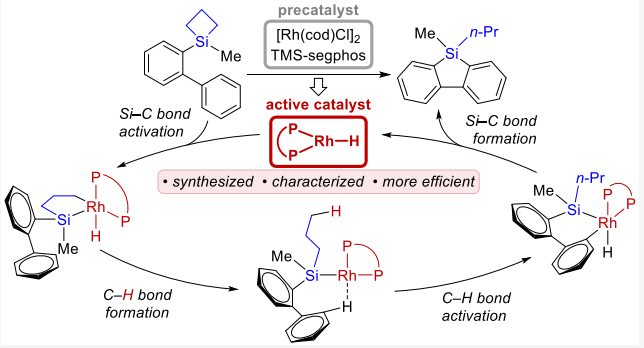

INTRODUCTION

Silicon-containing compounds are of paramount importance in organic synthesis, polymer science, and biological research.[1−8] Historically, silicon atoms were incorporated mainly via nucleophilic substitution of halosilanes[9,10] or hydrosilylation with hydrosilanes.[11−17] Over the past decades, catalytic direct silylation of C−H bonds has emerged as an attractive strategy that met with numerous progresses.[18−68] This new strategy not only embraces the widely conceived advantages of C−H functionalization[69−76] (C moiety) but also provides many more choices on silylation reagents (Si moiety). Such combinations of versatile C and Si moieties have greatly enhanced the complexity and diversity of silicon-containing compounds. To date, various silicon functionalities including hydrosilanes,[18−52] disilanes,[53−58] Si−B compounds,[59,60] and Si−C bonds[61−68] have been ingeniously devised as silylation reagents. However, the search and study of new C−H silylation reagents are still warranted as the available choices are far less than desired.

Silacyclobutanes (SCBs)[77] have been studied for a long time for their reactivity derived from their unique ring strain (Scheme 1). They were shown to suffer retro-[2 + 2] thermodecompositions that led to polymerization.[78] Due to their strain-release Lewis acidity, SCBs have also been employed in Mukaiyama aldol reactions[79,80] and Hiyama−Denmark cross-couplings.[81] The most interesting class of transformations of

Scheme 1. Transformations of SCBs

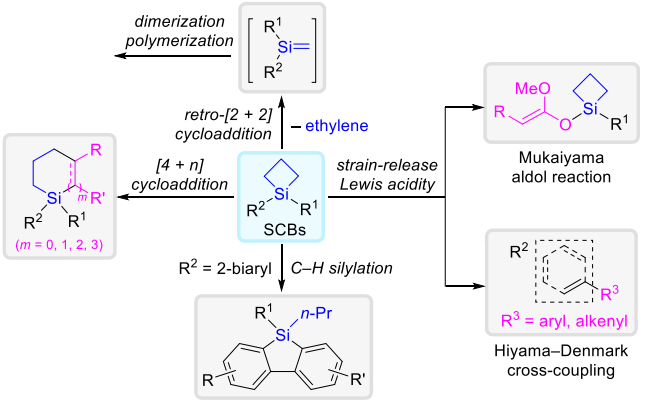

SCBs is perhaps transition-metal-catalyzed reactions with unsaturated carbon−carbon bonds or small-ring compounds,

Received: December 25, 2020
Published: February 23, 2021

https://dx.doi.org/10.1021/jacs.0c13335
J. Am. Chem. Soc. 2021, 143, 3571−3582

as manifested in either a ring-opening manner[82] or a formal cycloaddition manner.[83−92] These reactions are proposed to involve five-membered metallocycle intermediates via oxidative insertion into the SCBs, followed by the migratory insertion of the unsaturated carbon−carbon bonds to form ring-expansion intermediates. From there, the fates of the ring-expansion intermediates could diverge from β-hydride (β-H) elimination (ring-opening manner; giving acyclic products) to reductive elimination (cycloaddition manner; giving cyclic products). If chiral ligands were used, the cycloadditions could be rendered enantioselective to afford cyclic products chiral on the silicons.[83−86] Despite these interesting transformations, SCBs were not known to react with C−H bonds.

Recently, we reported for the first time that SCBs are efficient C−H silylation reagents under Rh catalysis (Scheme 2a).[93] We further employed a new chiral diphosphine ligand,

Scheme 2. Rh-Catalyzed C−H Silylation with SCBs

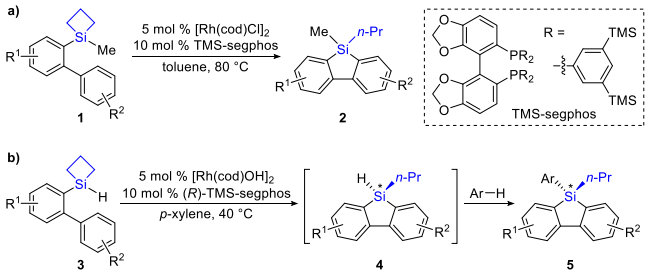

(*R*)-TMS-segophos that has a narrow dihedral angle and steric bulkiness, in the tandem SCB opening/C−H silylation reaction.[94] We successfully delivered a wide array of dibenzosiloles containing silicon-stereogenic centers with excellent enantioselectivities (up to 93% ee) (Scheme 2b). While our progresses opened up many possibilities to engage SCBs with different C−H reacting partners, conceivably in an intermolecular and enantioselective version, they also raised many fascinating questions. For example, why does C−H silylation become possible under our reaction conditions? What is the active catalytic species? What is the enantio-determining step? Why do aryl C−H bonds react faster than benzylic C−H bonds? To the best of our knowledge, mechanistic studies on C−H silylations mainly focused on hydrosilanes[95−102] and theoretical studies on SCBs focused on cycloadditions.[103−105] While the collective body of knowledge about C−H silylations is undoubtedly inspirational, the answers to the above questions are not readily clear. We thus strived to decode the puzzle to further capitalize the potential of SCBs and the Rh/diphosphine catalyst system in C−H silylations.

Herein, we report our combined computational and experimental mechanistic study on the Rh-catalyzed intramolecular C−H silylation with SCBs. We discovered that (1) [Rh]−H is probably the active catalytic species, as opposed to the previously proposed [Rh]−Cl; (2) [Rh]−H is generated via a reductive elimination/β-H elimination sequence, as opposed to the previously proposed endocyclic β-H elimination; and (3) the discretely synthesized and characterized [Rh]−H is a more efficient catalyst than the [Rh]−Cl. In addition, our results account well for the observed regio- and enantioselectivities. This work reconciles the difference between SCBs and hydrosilanes, echoing the pioneering studies from Hartwig[95,96] and Takai[99] groups. It also provides valuable insights and a useful catalyst system for future C−H silylation reactions.

RESULTS AND DISCUSSION

Previously Proposed Mechanism with [Rh]−Cl Catalyst. We proposed a possible reaction mechanism in ref 93 (Figure 1). The reaction initiates with the oxidative addition of

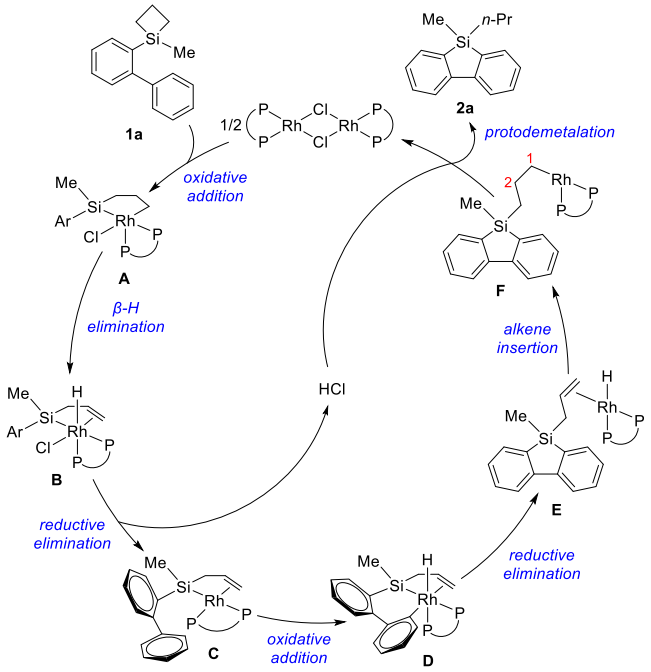

Figure 1. Proposed mechanism in ref 93. Diphosphine ligand = TMS-segphos. Ar = 2-biphenyl.

SCB substrate **1a** to Rh^I, generating five-membered rhodacycle **A**. An endocyclic β-H elimination[106,107] on **A** furnishes rhodium(III) hydride species **B**, which undergoes a subsequent reductive elimination to give intermediate **C** and HCl. Oxidative insertion of Rh^I into one aryl C−H bond of the biphenyl group in **C** generates rhodium(III) hydride intermediate **D**, followed by reductive elimination to form the Si−C bond. The resulting rhodium(I) hydride intermediate **E** undergoes an alkene insertion to form alkylrhodium species **F**. Finally, protodemetalation of **F** by HCl provides dibenzosilole product **2a** and completes the catalytic cycle. In such a catalytic cycle, the endocyclic β-H elimination was proposed since we observed deuterium scrambling on the C1 and C2 positions (see structure **F**).

To investigate the [Rh]−Cl mechanism, we selected the intramolecular C−H silylation of SCB **1a** in toluene as the model reaction for density functional theory (DFT) calculations (Figure 2; see Supporting Information for the complete free energy profile). The model catalyst $[Rh(\mathbf{L1})Cl]_2$ (**CAT1**) was used to simplify the computations. The [Rh]−Cl mechanism is initiated by the insertion of [Rh]−Cl into SCB **1a** via **TS1**. The resulting Rh^{III} intermediate **INT1** then proceeds through an endocyclic β-H elimination (via **TS2**) with an activation free energy of 14.8 kcal/mol. Such a Rh-involved endocyclic β-H elimination was not widely documented. We hypothesize that the big diphosphine ligand may render it possible. Then, reductive elimination (via **TS3**) takes place to give Rh^I intermediate **INT3**, which is the key

https://dx.doi.org/10.1021/jacs.0c13335
J. Am. Chem. Soc. 2021, 143, 3571−3582

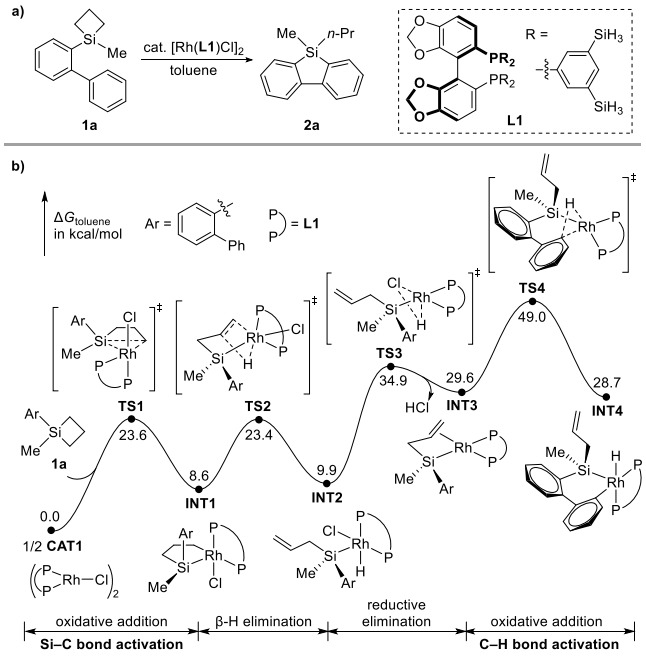

Figure 2. (a) Model reaction for DFT calculations. (b) Part of the free energy profile for the [Rh]−Cl mechanism. Computed at the SMD(toluene)/B3LYP-D3(BJ)/def2-TZVP-6-311++G(d,p)//B3LYP/LANL2DZ-6-31G(d) level.

intermediate for the subsequent rate-limiting C−H bond activation (via **TS4**). The overall activation free energy of the [Rh]−Cl mechanism is 49.0 kcal/mol (from **CAT1** to **TS4**), which is too high for a reaction that proceeds at 80 °C. Besides, the rate-limiting step, that is, the C−H bond activation step, is inconsistent with the kinetic isotope effect (KIE) observed in our previous study (1.0 for parallel reactions).[93] These results indicate that the [Rh]−Cl mechanism is not feasible and [Rh]−Cl may not be the real catalytic species.

Revised Mechanism with [Rh]−H as the Active Catalyst. Previously, the Hartwig group showed that the catalyst resting state in the Rh-catalyzed silylation of aryl C−H bonds was a five-coordinate silyl Rh^{III} complex.[95] Such a resting state could be reversibly converted to an active rhodium(I) hydride catalyst. [Rh]−H has also been proposed as the active species in Rh-catalyzed C−H silylation developed by Takai.[99] In addition, in our previously proposed mechanism, a tentative rhodium(I) hydride intermediate, that is, structure **E** in Figure 1, was also proposed. These threads led us to consider a scenario where a [Rh]−H species is the active catalyst. Thus, a revised mechanism involving the generation of the active [Rh]−H catalyst and the catalytic cycle of C−H silylation has been proposed.

Generation of [Rh]−H. The generation of the dimeric [Rh]−H species $[Rh(\mathbf{L1})H]_2$ (**CAT2**) was first studied (Figure 3). The reaction starts with the dissociation and insertion of the catalyst into substrate **1a** to form five-membered silametallacycle **INT1** via **TS1** with an activation free energy of 23.6 kcal/mol. Subsequently, reductive elimination (via **TS5**) and β-H elimination (via **TS6**) occur to form the active catalyst dimer **CAT2** and chlorosilane **6a** (see Supporting Information for experimental attempts to detect chlorosilane **6a** or its derivatives). The overall free energy barrier is 25.6 kcal/mol (from **CAT1** to **TS5**).

There exists another pathway involving a different reaction sequence (see the red line in Figure 3). Silametallacycle **INT1** may first undergo endocyclic β-H elimination via **TS2**. The resulting intermediate **INT2** then proceeds through a reductive elimination process via **TS7** to generate **INT7**, which dimerizes to furnish the dimeric species **CAT2**. The overall

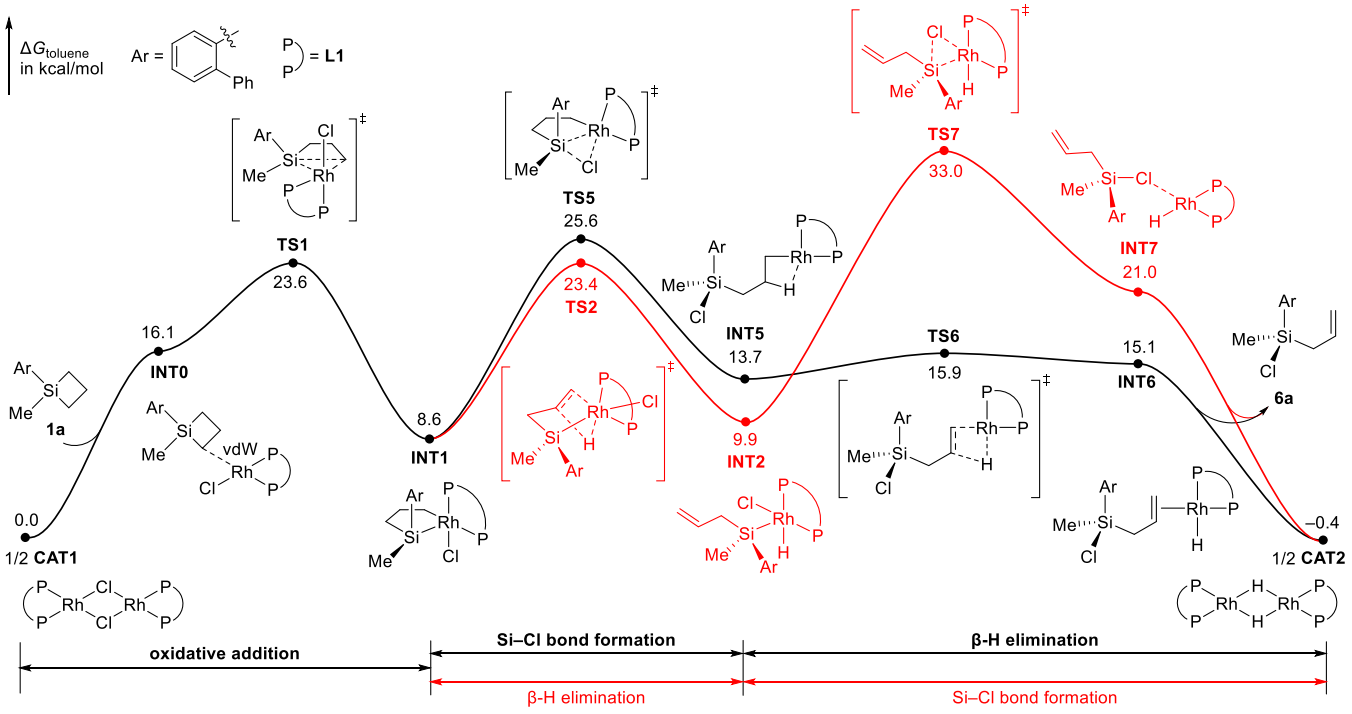

Figure 3. Free energy profile for the generation of [Rh]−H species **CAT2**. Computed at the SMD(toluene)/B3LYP-D3(BJ)/def2-TZVP-6-311++G(d,p)//B3LYP/LANL2DZ-6-31G(d) level.

https://dx.doi.org/10.1021/jacs.0c13335
J. Am. Chem. Soc. 2021, 143, 3571−3582

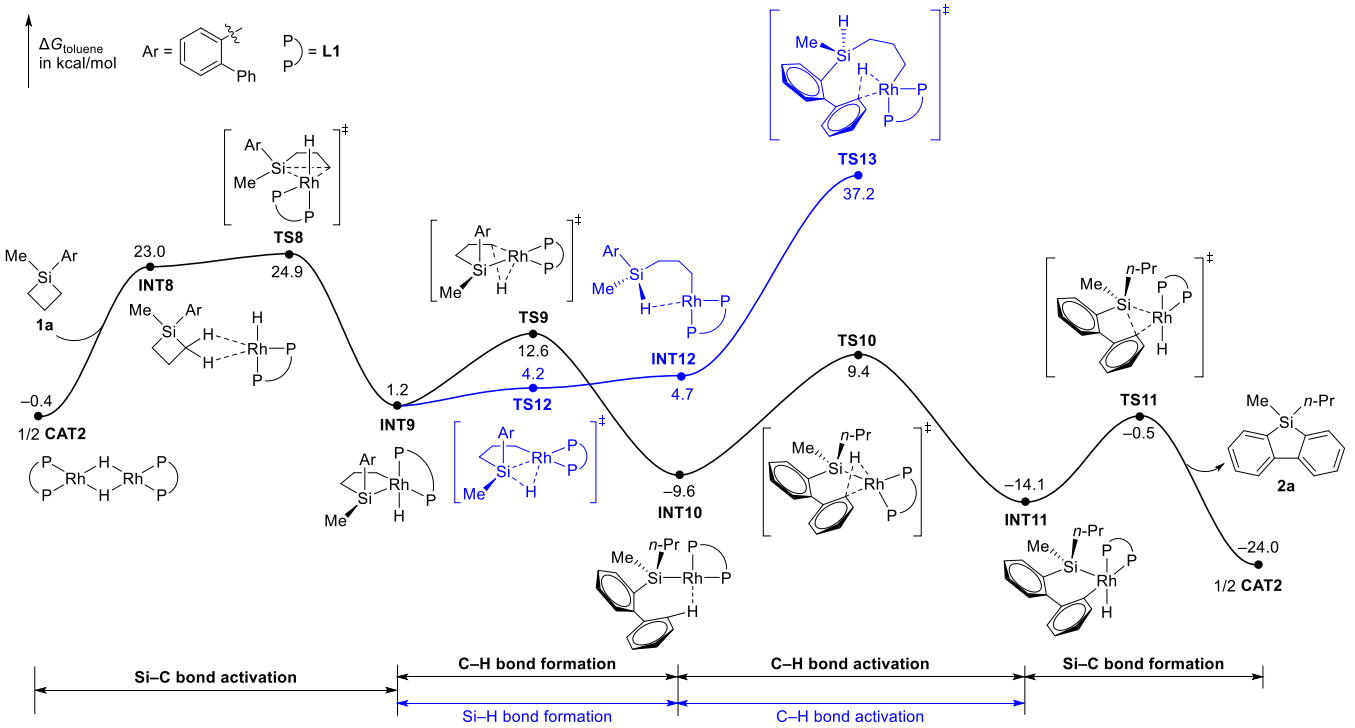

Figure 4. Free energy profile for the catalytic cycle of the [Rh]−H mechanism. Computed at the SMD(toluene)/B3LYP-D3(BJ)/def2-TZVP-6-311++G(d,p)//B3LYP/LANL2DZ-6-31G(d) level.

activation free energy for this pathway is as high as 33.0 kcal/mol (from **CAT1** to **TS7**) and thus energetically unfavorable.

Catalytic Cycle of C−H Silylation. After the generation of the active [Rh]−H catalyst, the catalytic cycle shown in Figure 4 is initiated. The active catalyst [Rh]−H first undergoes oxidative insertion into SCB **1a** via **TS8**. Then, reductive elimination of **INT9** overcomes a free energy barrier of 11.4 kcal/mol via **TS9** to form Rh^{I} intermediate **INT10**. The subsequent C−H bond activation (via **TS10**) and reductive elimination (via **TS11**) are calculated to be facile, providing product **2a** and regenerating the [Rh]−H species. For **INT11**, the reverse C−H bond formation (via **TS10**) is out-competed by the forward Si−C bond formation (via **TS11**). Therefore, the C−H bond activation step (from **INT10** to **INT11**) is irreversible. The overall activation free energy for the catalytic cycle is 25.3 kcal/mol (from **CAT2** to **TS8**), showing that this reaction is energetically feasible.

Since only Rh^{I} can undergo C−H bond activation via oxidative addition, another possible mechanism for the conversion of the Rh^{III} intermediate **INT9** to Rh^{I} intermediate **INT12** is also studied (blue line in Figure 4). Reductive elimination of **INT9** via **TS12** experiences a small free energy barrier of 3.0 kcal/mol to give **INT12**. However, the free energy barrier for the subsequent C−H bond activation via **TS13** is much higher than that for **TS9** (37.2 kcal/mol versus 12.6 kcal/mol), suggesting that this mechanism is unlikely to be operative.

DFT Calculations on the Regio- and Enantioselectivities. Next, we examined whether the revised mechanism could account for the previously observed regio- and enantioselectivities (Figure 5a). When substrate **1b** with an *ortho*-methyl group was used, both $C(sp^2)$−H and $C(sp^3)$−H silylation products **2b** and **7b** were observed in a ratio of 1:0.7.[93] The competition of $C(sp^2)$−H versus $C(sp^3)$−H bonds was studied by comparing the relative free energies of the C−H bond activation transition states (Figure 5b). DFT calculations indicate that the $C(sp^2)$−H bond activation transition state **TS14-sp²** is favored over the $C(sp^3)$−H bond activation transition state **TS14-sp³** by only 0.4 kcal/mol, suggesting that products **2b** and **7b** should be formed with comparable yields. This is consistent with the experimental findings.

Our mechanistic study reveals that the oxidative addition of SCBs (e.g., **TS8** in Figure 4) is the enantio-determining step. Here we use the 2-biphenyl substrate **3a**, Rh[(*R*)-TMS-segphos]H, and toluene as the model system to investigate the origins of enantioselectivity (Figure 5a). DFT calculations suggest two geometries **TS15-*S*** and **TS15-*R*** as the most favored transition states to generate (*S*)- and (*R*)-products, respectively (Figure 5c; here we suppose A-ring > B-ring > *n*-Pr > H to differentiate the absolute configurations). Generation of (*S*)-**4a** via **TS15-*S*** is kinetically favored over the formation of (*R*)-**4a** via **TS15-*R*** by 2.2 kcal/mol in terms of free energies, which is in line with the experimental observations.[94] DFT calculations indicate that the steric interaction plays a crucial role in the geometrical arrangement of the transition states. The steric map of the catalyst in a Quadrant projection,[108,109] which is viewed along the C_2-axis, shows the asymmetry of the catalytic pocket: The quadrants II and IV are almost completely blocked by the aryl groups (Figure 5d). This catalytic pocket explains that **TS15-*R*** is disfavored because the substrate places the SCB part into the most sterically hindered quadrant IV of the steric map. In addition, the interaction between the substrate and the rhodium catalyst may also affect the enatioselectivity. In **TS15-*S***, the substrate has a stronger interaction with the catalyst via a Rh···H−Si interaction (the Rh···H distance is 2.29 Å), which makes **TS15-*S*** favored over **TS15-*R***. The Liu, Buchwald, and Hartwig groups have attributed the superior enantioselectivity imposed by segphos-type ligands to

https://dx.doi.org/10.1021/jacs.0c13335
J. Am. Chem. Soc. 2021, 143, 3571−3582

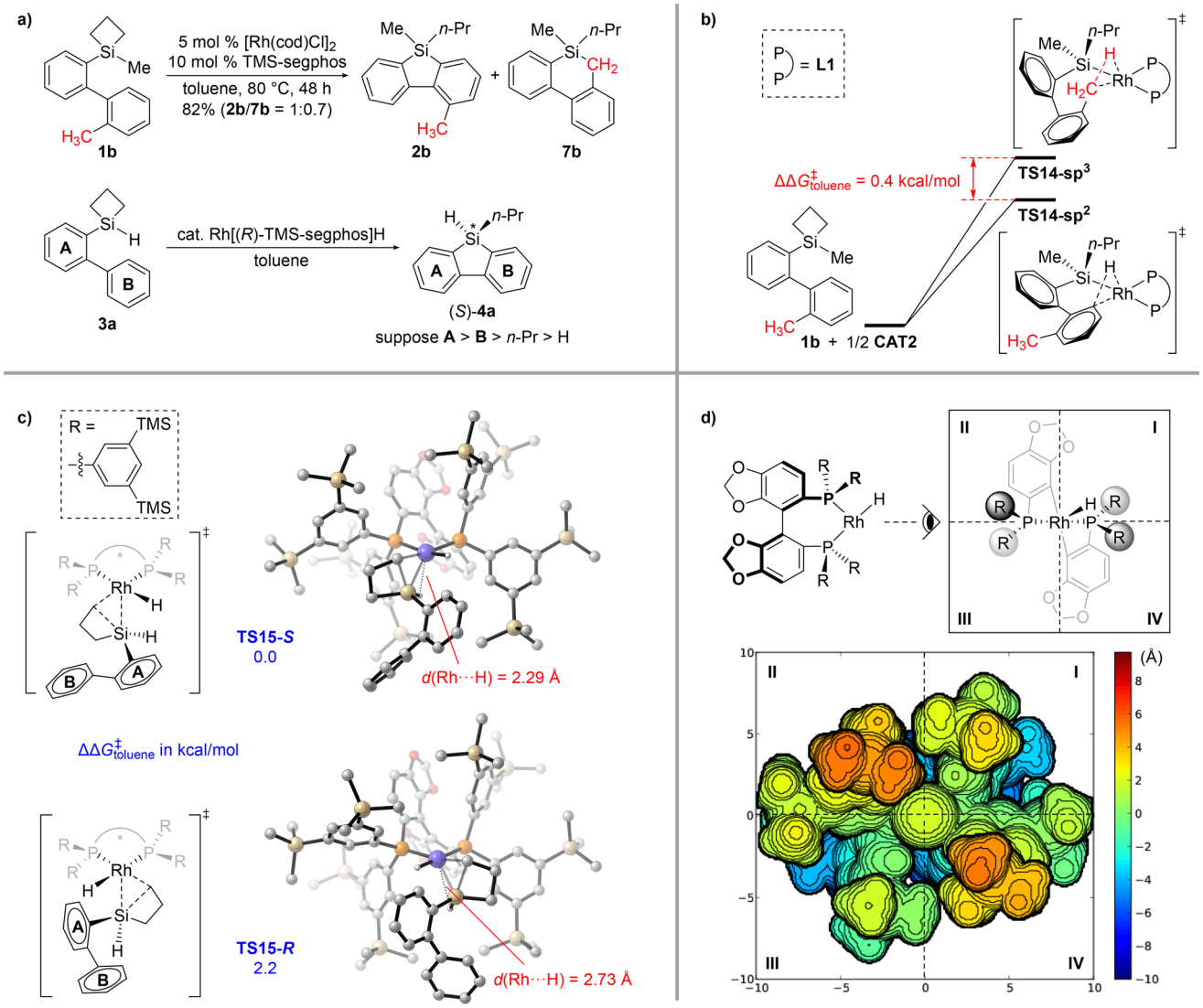

Figure 5. (a) Reactions for studing selectivities. (b) Activation of C(sp^2)−H and C(sp^3)−H bonds of substrate **1b**. (c) Geometries and relative free energies of Si−C bond activation transition states **TS15-*S*** and **TS15-*R***. (d) Quadrant projection of Rh[(*R*)-TMS-segphos]H and the corresponding steric map in Quadrant projection. Computed at the SMD(toluene)/B3LYP-D3(BJ)/def2-TZVP-6-311++G(d,p)//B3LYP/LANL2DZ-6-31G(d) level.

attractive ligand−substrate dispersion.[110,111] However, in our case, energy decomposition analysis[112,113] suggests that the steric interactions and the resulting distortion of the catalyst rather than dispersion interactions determine the enantioselectivity (see Supporting Information for details).

Experimental Mechanistic Study with [Rh]−H. Our computations provide valuable mechanistic information that a [Rh]−H species generated in situ is likely the active catalytic species of the reaction. We reinvestigated the kinetic behavior of C−H silylation under [Rh]−Cl catalysis by ^{1}H NMR analysis, finding that the silylation reaction involves two stages: an induction period (∼1 h at 40 °C) and an active period featuring faster consumption of the substrate (see Supporting Information for details). The unambiguous observation of the induction period motivated us to carry out numerous experiments to confirm the Rh−H catalysis and to explore the possible advantages of [Rh]−H-catalyzed reactions considering that using [Rh]−H as the catalyst would avoid such an induction period and possible side reactions caused by [Rh]−Cl in the induction period. To this end, we synthesized and characterized the discrete [Rh]−H catalyst, then used them toward mechanistic and utility studies.

Synthesis and Characterization of [Rh]−H. The reaction between $[Rh(C_2H_4)_2Cl]_2$ with 2.0 equiv of TMS-segphos failed to generate dimeric $[Rh(TMS\text{-}segphos)Cl]_2$ (see Supporting Information for details). We observed that only half of the presumably labile ethylene was displaced by the diphosphine, which was surprising and rarely documented.[114] We speculated that the large steric hindrance of our diphosphine ligand might be the problem. Instead, the rhodium hydride complex $[(TMS\text{-}segphos)Rh(\mu_2\text{-}H)_2Rh(C_2H_4)_2]$ (**CAT3**) was prepared in situ from $[Rh(C_2H_4)_2Cl]_2$/TMS-segphos and excess triethylsilane (Scheme 3). The rhodium hydride species was substantiated by ^{1}H and ^{31}P NMR spectroscopy as well as HRMS analysis (see Supporting Information for details). Of note, a characteristic hydride signal at −7.36 ppm was observed in the ^{1}H NMR spectrum.

Measurement of KIEs. To determine whether the C−H bond activation step in the catalytic cycle is rate-limiting,

https://dx.doi.org/10.1021/jacs.0c13335
J. Am. Chem. Soc. 2021, 143, 3571−3582

Scheme 3. Synthesis of Rhodium Hydride Complex CAT3

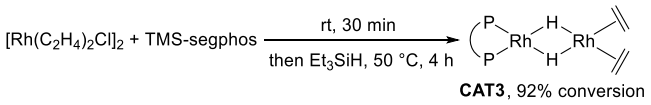

substrates **1a** and **1a-d_5** were treated with **CAT3** in separate NMR tubes and monitored by ^{1}H NMR spectroscopy (Scheme 4a). The measured KIE was 1.0, indicating that the

Scheme 4. Deuterium-Labeling Experiments[a]

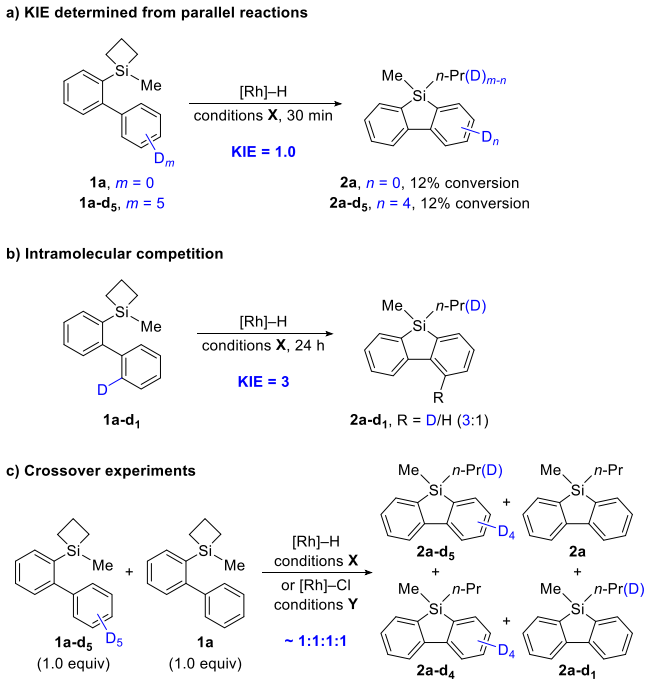

[a]Conditions X: Substrate(s) (0.1 mmol, 1.0 equiv), 2 mol % **CAT3**, 40 °C. Conditions Y: **1a-d_5** (0.1 mmol, 1.0 equiv), **1a** (0.1 mmol, 1.0 equiv), 5 mol % [Rh(cod)Cl]$_2$, 10 mol % TMS-segphos, 80 °C.

cleavage of aryl C−H bond is not rate-limiting. This experimental observation is consistent with our computational results. In addition, the intramolecular competition experiment was conducted with **1a-d_1** as the substrate (Scheme 4b). A ratio of 3:1 (C−H versus C−D activation) was observed, and the same ratio was recorded when [Rh]−Cl was utilized.[93]

Crossover Experiments. SCBs **1a** and **1a-d_5** (0.1 mmol each) were treated under [Rh]−H and [Rh]−Cl catalysis, respectively (Scheme 4c). Both reactions were quenched at <10% conversion, and the reaction mixtures were analyzed by GC-MS. An almost even distribution of four possible molecular weights corresponding to all of the four possible products in Scheme 4c was observed, which is consistent with our computational results that [Rh]−H species participates in the catalytic cycle in an intermolecular manner ([Rh]−H formed in the final stage of a catalytic cycle will incorporate the metal-bound hydrogen atom into the *n*-Pr group of the product of the next cycle) as opposed to an intramolecular manner.

Kinetic Measurements. We monitored the reaction of SCB **1a** under [Rh]−H catalysis by ^{1}H NMR analysis (Figure 6a). In contrast to the reaction conducted with [Rh]−Cl, no induction period was observed in this case. The rate law of the reaction was then acquired from the reaction profiles, showing

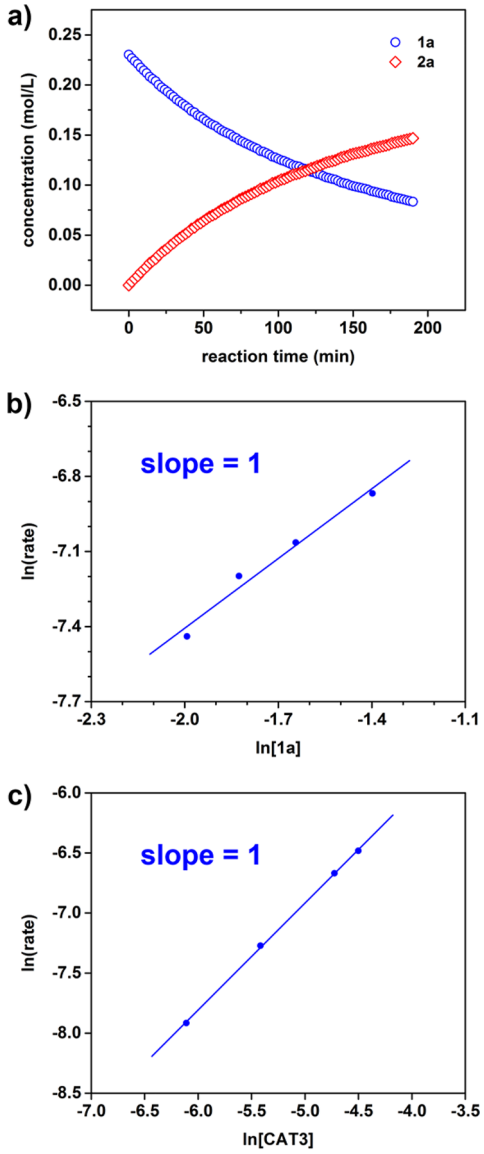

Figure 6. Kinetic experiments. (a) Kinetic profile of the intramolecular C−H silylation of **1a** with **CAT3** as the catalyst. (b) Determination of the reaction order in **1a**. (c) Determination of the reaction order in **CAT3**. See Supporting Information for details.

that the reaction was first order in both the substrate (Figure 6b) and [Rh]−H (Figure 6c). An Arrhenius plot in a temperature range from 30 to 50 °C revealed the activation energy (E_a) to be 23.4 kcal/mol (see Supporting Information for details). Fitting the obtained reaction rates to the Eyring equation determined the activation parameters of $\Delta H^{\ddagger}$ = 22.8 kcal/mol and $\Delta S^{\ddagger}$ = 13.5 cal/(mol·K).

[Rh]−H Is a More Efficient Catalyst. Consistent with our predictions, we were delighted to witness that [Rh]−H was a better catalyst than [Rh]−Cl. The reaction under [Rh]−H catalysis takes place at a lower temperature and at a lower catalyst loading, yet affords a better yield (Table 1). For example, the intramolecular C−H silylation of SCB **1a** proceeded smoothly at 40 °C with 2 mol % **CAT3**, generating product **2a** in an excellent 95% yield (Table 1, entry 2). Under the same set of conditions, the conversion under [Rh]−Cl catalysis was meager (24%) with most of the substrate remained (Table 1, entry 1). The reaction even proceeded at

https://dx.doi.org/10.1021/jacs.0c13335
J. Am. Chem. Soc. 2021, 143, 3571−3582

Table 1. Evaluation of Catalytic Efficiency[a]

entry	reaction conditions	conversion (%)
1	5 mol % $[Rh(C_2H_4)_2Cl]_2$, 10 mol % TMS-segphos	24
2	2 mol % **CAT3**	97 (95[b])
3[c]	10 mol % **CAT3**	26
4	5 mol % $[Rh(C_2H_4)_2Cl]_2$, 1 equiv of Et_3SiH	ND

[a]Reactions were conducted with **1a** (0.1 mmol) in toluene (1.0 mL) at 40 °C for 24 h. The conversion was determined by ^{1}H NMR analysis. [b]Isolated yield. [c]Reaction was conducted at 0 °C. ND = not detected.

0 °C with 10 mol % **CAT3**, reaching 26% conversion after 24 h (Table 1, entry 3). No reaction took place in the absence of the diphosphine ligand (Table 1, entry 4), suggesting that background reaction without a ligand is not operative. The finding of no background reaction is especially encouraging in terms of designing enantioselective silylation using SCBs.

The superiority of the [Rh]−H catalysis is further demonstrated by the intramolecular C−H silylation of 12 representative SCBs (Table 2). The reaction yields under [Rh]−H catalysis are compared head to head to those under [Rh]−Cl catalysis. It is clear that [Rh]−H is more efficient across the panel, especially on the substrates that are resistant to [Rh]−Cl conditions (e.g., **2c−e** and **2n**). In addition, we were delighted to observe that aryl−halide bonds (e.g., **2i** and **2j**) remained compatible with [Rh]−H catalysis, which is an advantage over Pd catalysis.

Summary of the [Rh]−H Mechanism. For clarity and completeness, we offer a summary of the [Rh]−H mechanism (Figure 7) based on our computational and experimental results as well as literature findings.[95−105] First, coordination of substrate **1a** to the rhodium catalyst occurs. The resulting intermediate **G** undergoes Si−C bond activation via oxidative addition to generate Rh^{III} intermediate **H**, which then proceeds through C−H bond formation via reductive elimination to give silylrhodium(I) species **I**. Subsequently, Rh^{I}-mediated C−H bond activation leads to the Rh^{III} intermediate **J**. Finally, reductive elimination and catalyst transfer furnish dibenzosilole product **2a** and complete the catalytic cycle. When [Rh]−Cl was used as the precatalyst, we suggest that [Rh]−Cl might first react with substrate **1a** to generate intermediate **G** through the reaction pathway shown in Figure 3.

CONCLUSION

Based on computational results, experimental observations, and literature findings, we propose that [Rh]−H in situ generated from [Rh]−Cl during the induction period is the active catalyst for Rh-catalyzed intramolecular C−H silylation with SCBs. The catalytic cycle consists of Si−C bond activation, C−H bond formation, C−H bond activation, and Si−C bond formation steps. The key C−H bond activation step is irreversible but not rate limiting. This mechanism accounts well for the observed regio- and enantioselectivities. Importantly, our experiments with discretely synthesized [Rh]−H are fully consistent with the [Rh]−H catalytic cycle and demonstrate that [Rh]−H is a more efficient catalyst in terms of reaction rates and yields. This study is a good example that collaboration between dry and wet laboratories sheds light on the reaction mechanism and streamlines the catalyst system. It also showcases the guiding role of computations as manifested in the course of detecting reaction intermediates (e.g., **6a**) and proposing new catalysts (e.g., [Rh]−H). Taking advantage of the more reactive [Rh]−H catalyst, we are actively pursuing the first examples of asymmetric intermolecular C−H silylation reactions on SCBs and shall report the results soon.

Table 2. Scope of [Rh]−H-Catalyzed C−H Silylation[a]

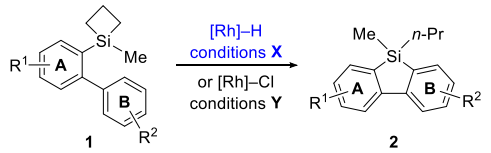

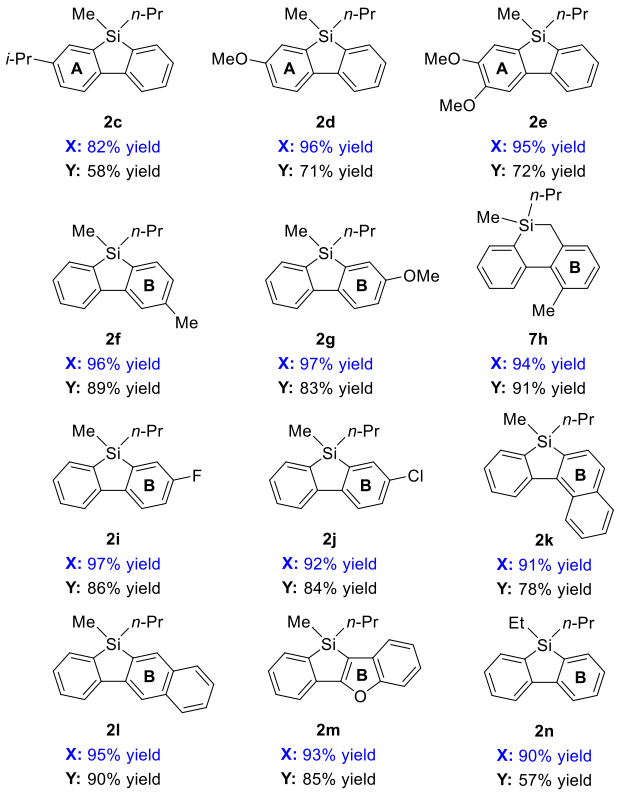

[a]Reactions were conducted with **1** (0.1 mmol) in toluene (1.0 mL). The yields refer to isolated yields. Conditions X: 2 mol % (with substituent(s) at B-ring) or 5 mol % (with substituent(s) at A-ring) **CAT3**, 40 °C, 24 h. Conditions Y: 5 mol % $[Rh(cod)Cl]_2$, 10 mol % TMS-segphos, 80 °C, 48 or 72 h; yields have been previously reported in ref 93.

COMPUTATIONAL METHODS

Geometry optimizations were performed in the gas phase using B3LYP functional[115,116] with the Gaussian 09 program package.[117] Pople's double-ζ basis set 6-31G(d) was adopted for H, C, O, Si, P, and Cl atoms.[118] For Rh, the LANL2DZ basis set with effective core potential (ECP) was employed.[119] Frequency analyses were performed at the same level to obtain thermal corrections at 298 K and to confirm the stationary points with zero imaginary frequency and transition states with only one imaginary frequency. Solution-phase single-point refinements in toluene were calculated using the SMD solvation model,[120] B3LYP functional with Grimme's D3(BJ) dispersion,[121,122] and a mixed basis set, in which the triple-ζ basis set 6-311++G(d,p) was used for H, C, O, Si, P, and Cl atoms[118] and the def2-TZVP basis set[123] with ECP[124] was used for Rh. All discussed energy differences were based on free energies at 298 K (standard states are the hypothetical states at 1 mol/L). For structures with

https://dx.doi.org/10.1021/jacs.0c13335
J. Am. Chem. Soc. 2021, 143, 3571−3582

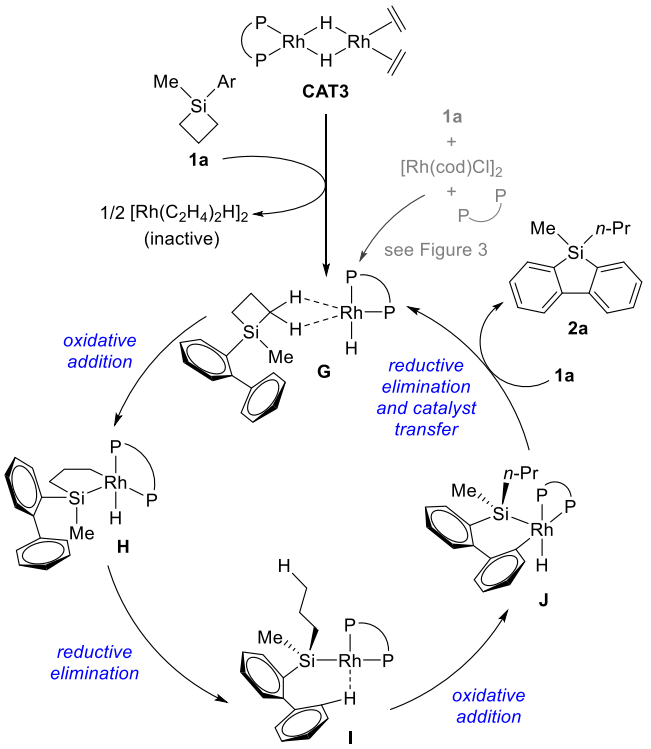

Figure 7. Refined [Rh]−H mechanism. Diphosphine ligand = TMS-segphos.

ligand **L1**, a conformational search was first performed with segphos. Then, silyl groups were added to a few low-energy conformers, and the geometries were reoptimized. For **TS15-*S*** and **TS15-*R***, the conformational search was directly carried out with TMS-segphos. Generalized Kohn−Sham energy decomposition analysis[112,113] was performed with GAMESS.[125] Three-dimensional structures were prepared with CYLview.[126] The steric map for analyzing catalytic pocket was built with SambVca 2.[127−129]

B3LYP-D3 functional has been widely applied in the theoretical studies on Rh-catalyzed reactions.[99,130−133] To further examine the reliability of our computations with B3LYP-D3(BJ), we compared the computed overall activation free energies and selectivities with three other popular density functionals, namely, PBE0-D3(BJ),[121,122,134] M06,[135] and ωB97X-D,[136] finding that different functionals exhibited consistent trends (see Supporting Information for details).

■ ASSOCIATED CONTENT

Supporting Information

The Supporting Information is available free of charge at https://pubs.acs.org/doi/10.1021/jacs.0c13335.

Computational details, experimental procedures, characterization data, and copies of NMR spectra (PDF)

■ AUTHOR INFORMATION

Corresponding Authors

Xinhao Zhang − *Lab of Computational Chemistry and Drug Design, State Key Laboratory of Chemical Oncogenomics, Peking University Shenzhen Graduate School, Shenzhen 518055, China; Shenzhen Bay Laboratory, Shenzhen 518055, China;* orcid.org/0000-0002-8210-2531; Email: zhangxh@pkusz.edu.cn

Zhi-Xiang Yu − *Beijing National Laboratory for Molecular Sciences (BNLMS), Key Laboratory of Bioorganic Chemistry and Molecular Engineering of Ministry of Education, College of Chemistry, Peking University, Beijing 100871, China; Shenzhen Bay Laboratory, Shenzhen 518055, China;* orcid.org/0000-0003-0939-9727; Email: yuzx@pku.edu.cn

Wei He − *MOE Key Laboratory of Bioorganic Phosphorus Chemistry and Chemical Biology and School of Pharmaceutical Sciences and Tsinghua-Peking Joint Centers for Life Sciences, Tsinghua University, Beijing 100084, China;* orcid.org/0000-0001-8167-9155; Email: whe@mail.tsinghua.edu.cn

Authors

Linxing Zhang − *Lab of Computational Chemistry and Drug Design, State Key Laboratory of Chemical Oncogenomics, Peking University Shenzhen Graduate School, Shenzhen 518055, China*

Kun An − *MOE Key Laboratory of Bioorganic Phosphorus Chemistry and Chemical Biology and School of Pharmaceutical Sciences and Tsinghua-Peking Joint Centers for Life Sciences, Tsinghua University, Beijing 100084, China;* orcid.org/0000-0002-2595-9803

Yi Wang − *Beijing National Laboratory for Molecular Sciences (BNLMS), Key Laboratory of Bioorganic Chemistry and Molecular Engineering of Ministry of Education, College of Chemistry, Peking University, Beijing 100871, China;* orcid.org/0000-0001-5762-5958

Yun-Dong Wu − *Lab of Computational Chemistry and Drug Design, State Key Laboratory of Chemical Oncogenomics, Peking University Shenzhen Graduate School, Shenzhen 518055, China; Beijing National Laboratory for Molecular Sciences (BNLMS), Key Laboratory of Bioorganic Chemistry and Molecular Engineering of Ministry of Education, College of Chemistry, Peking University, Beijing 100871, China; Shenzhen Bay Laboratory, Shenzhen 518055, China;* orcid.org/0000-0003-4477-7332

Complete contact information is available at: https://pubs.acs.org/10.1021/jacs.0c13335

Author Contributions

#These authors contributed equally.

Notes

The authors declare no competing financial interest.

■ ACKNOWLEDGMENTS

This work was supported by the National Natural Science Foundation of China (21625104, 21901235, 21933003, 21933004, 21971133, and 91856105), the Shenzhen STIC (JCYJ20170412150343516), and High-Performance Computing Platform of Peking University. We thank Prof. Peifeng Su (Xiamen University) and Dr. Yuezhi Mao (Stanford University) for their assistance in energy decomposition analysis.

■ REFERENCES

(1) Cheng, C.; Hartwig, J. F. Catalytic Silylation of Unactivated C−H Bonds. *Chem. Rev.* **2015**, *115*, 8946−8975.

(2) Yang, Y.; Wang, C. Direct Silylation Reactions of Inert C−H Bonds via Transition Metal Catalysis. *Sci. China: Chem.* **2015**, *58*, 1266−1279.

(3) Shang, X.; Liu, Z.-Q. Recent Developments in Free-Radical-Promoted C−Si Formation via Selective C−H/Si−H Functionalization. *Org. Biomol. Chem.* **2016**, *14*, 7829−7831.

(4) Omann, L.; Königs, C. D. F.; Klare, H. F. T.; Oestreich, M. Cooperative Catalysis at Metal−Sulfur Bonds. *Acc. Chem. Res.* **2017**, *50*, 1258−1269.
(5) Parasram, M.; Gevorgyan, V. Silicon-Tethered Strategies for C−H Functionalization Reactions. *Acc. Chem. Res.* **2017**, *50*, 2038−2053.
(6) Komiyama, T.; Minami, Y.; Hiyama, T. Recent Advances in Transition-Metal-Catalyzed Synthetic Transformations of Organosilicon Reagents. *ACS Catal.* **2017**, *7*, 631−651.
(7) Bähr, S.; Oestreich, M. Electrophilic Aromatic Substitution with Silicon Electrophiles: Catalytic Friedel−Crafts C−H Silylation. *Angew. Chem., Int. Ed.* **2017**, *56*, 52−59.
(8) Wilkinson, J. R.; Nuyen, C. E.; Carpenter, T. S.; Harruff, S. R.; Van Hoveln, R. Copper-Catalyzed Carbon−Silicon Bond Formation. *ACS Catal.* **2019**, *9*, 8961−8979.
(9) Lalonde, M.; Chan, T. H. Use of Organosilicon Reagents as Protective Groups in Organic Synthesis. *Synthesis* **1985**, *1985*, 817−845.
(10) Kyushin, S. Organosilicon Synthesis for Construction of Organosilicon Clusters. In *Efficient Methods for Preparing Silicon Compounds*; Elsevier: Amsterdam, 2016; pp 455−498.
(11) Díez-González, S.; Nolan, S. P. Copper, Silver, and Gold Complexes in Hydrosilylation Reactions. *Acc. Chem. Res.* **2008**, *41*, 349−358.
(12) Troegel, D.; Stohrer, J. Recent Advances and Actual Challenges in Late Transition Metal Catalyzed Hydrosilylation of Olefins from an Industrial Point of View. *Coord. Chem. Rev.* **2011**, *255*, 1440−1459.
(13) Marciniec, B. *Comprehensive Handbook on Hydrosilylation*; Elsevier: Amsterdam, 2013.
(14) Nakajima, Y.; Shimada, S. Hydrosilylation Reaction of Olefins: Recent Advances and Perspectives. *RSC Adv.* **2015**, *5*, 20603−20616.
(15) Marciniec, B.; Maciejewski, H.; Pawluć, P. Hydrosilylation of Carbon−Carbon Multiple Bonds—Application in Synthesis and Materials Science. In *Organosilicon Compounds*; Elsevier: Amsterdam, 2017; pp 169−217.
(16) Du, X.; Huang, Z. Advances in Base-Metal-Catalyzed Alkene Hydrosilylation. *ACS Catal.* **2017**, *7*, 1227−1243.
(17) de Almeida, L. D.; Wang, H.; Junge, K.; Cui, X.; Beller, M. Recent Advances in Catalytic Hydrosilylations: Developments beyond Traditional Platinum Catalysts. *Angew. Chem., Int. Ed.* **2021**, *60*, 550−565.
(18) Gustavson, W. A.; Epstein, P. S.; Curtis, M. D. Homogeneous Activation of the C−H Bond. Formation of Phenylsiloxanes from Benzene and Silicon Hydrides. *Organometallics* **1982**, *1*, 884−885.
(19) Uchimaru, Y.; El Sayed, A. M. M.; Tanaka, M. Selective Arylation of a Si−H Bond in *o*-Bis(dimethylsilyl)benzene via C−H Bond Activation of Arenes. *Organometallics* **1993**, *12*, 2065−2069.
(20) Djurovich, P. I.; Dolich, A. R.; Berry, D. H. Transfer Dehydrogenative Coupling of Triethylsilane Catalysed by Ruthenium and Rhodium Complexes. A New Si−C Bond Forming Process. *J. Chem. Soc., Chem. Commun.* **1994**, 1897−1898.
(21) Kakiuchi, F.; Igi, K.; Matsumoto, M.; Chatani, N.; Murai, S. Ruthenium-Catalyzed Dehydrogenative Silylation of Aryloxazolines with Hydrosilanes via C−H Bond Cleavage. *Chem. Lett.* **2001**, *30*, 422−423.
(22) Tsukada, N.; Hartwig, J. F. Intermolecular and Intramolecular, Platinum-Catalyzed, Acceptorless Dehydrogenative Coupling of Hydrosilanes with Aryl and Aliphatic Methyl C−H Bonds. *J. Am. Chem. Soc.* **2005**, *127*, 5022−5023.
(23) Lu, B.; Falck, J. R. Efficient Iridium-Catalyzed C−H Functionalization/Silylation of Heteroarenes. *Angew. Chem., Int. Ed.* **2008**, *47*, 7508−7510.
(24) Ihara, H.; Suginome, M. Easily Attachable and Detachable *ortho*-Directing Agent for Arylboronic Acids in Ruthenium-Catalyzed Aromatic C−H Silylation. *J. Am. Chem. Soc.* **2009**, *131*, 7502−7503.
(25) Furukawa, S.; Kobayashi, J.; Kawashima, T. Development of a Sila-Friedel−Crafts Reaction and Its Application to the Synthesis of Dibenzosilole Derivatives. *J. Am. Chem. Soc.* **2009**, *131*, 14192−14193.
(26) Ureshino, T.; Yoshida, T.; Kuninobu, Y.; Takai, K. Rhodium-Catalyzed Synthesis of Silafluorene Derivatives via Cleavage of Silicon−Hydrogen and Carbon−Hydrogen Bonds. *J. Am. Chem. Soc.* **2010**, *132*, 14324−14326.
(27) Klare, H. F. T.; Oestreich, M.; Ito, J.-i.; Nishiyama, H.; Ohki, Y.; Tatsumi, K. Cooperative Catalytic Activation of Si−H Bonds by a Polar Ru−S Bond: Regioselective Low-Temperature C−H Silylation of Indoles under Neutral Conditions by a Friedel−Crafts Mechanism. *J. Am. Chem. Soc.* **2011**, *133*, 3312−3315.
(28) Oyamada, J.; Nishiura, M.; Hou, Z. Scandium-Catalyzed Silylation of Aromatic C−H Bonds. *Angew. Chem., Int. Ed.* **2011**, *50*, 10720−10723.
(29) Simmons, E. M.; Hartwig, J. F. Catalytic Functionalization of Unactivated Primary C−H Bonds Directed by an Alcohol. *Nature* **2012**, *483*, 70−73.
(30) Kuninobu, Y.; Nakahara, T.; Takeshima, H.; Takai, K. Rhodium-Catalyzed Intramolecular Silylation of Unactivated C-(sp^3)−H Bonds. *Org. Lett.* **2013**, *15*, 426−428.
(31) Cheng, C.; Hartwig, J. F. Rhodium-Catalyzed Intermolecular C−H Silylation of Arenes with High Steric Regiocontrol. *Science* **2014**, *343*, 853−857.
(32) Curless, L. D.; Ingleson, M. J. $B(C_6F_5)_3$-Catalyzed Synthesis of Benzofused-Siloles. *Organometallics* **2014**, *33*, 7241−7246.
(33) Ghavtadze, N.; Melkonyan, F. S.; Gulevich, A. V.; Huang, C.; Gevorgyan, V. Conversion of 1-Alkenes into 1,4-Diols through an Auxiliary-Mediated Formal Homoallylic C−H Oxidation. *Nat. Chem.* **2014**, *6*, 122−125.
(34) Li, B.; Driess, M.; Hartwig, J. F. Iridium-Catalyzed Regioselective Silylation of Secondary Alkyl C−H Bonds for the Synthesis of 1,3-Diols. *J. Am. Chem. Soc.* **2014**, *136*, 6586−6589.
(35) Toutov, A. A.; Liu, W.-B.; Betz, K. N.; Fedorov, A.; Stoltz, B. M.; Grubbs, R. H. Silylation of C−H Bonds in Aromatic Heterocycles by an Earth-Abundant Metal Catalyst. *Nature* **2015**, *518*, 80−84.
(36) Leifert, D.; Studer, A. 9-Silafluorenes via Base-Promoted Homolytic Aromatic Substitution (BHAS) − The Electron as a Catalyst. *Org. Lett.* **2015**, *17*, 386−389.
(37) Ma, Y.; Wang, B.; Zhang, L.; Hou, Z. Boron-Catalyzed Aromatic C−H Bond Silylation with Hydrosilanes. *J. Am. Chem. Soc.* **2016**, *138*, 3663−3666.
(38) Chen, Q.-A.; Klare, H. F. T.; Oestreich, M. Brønsted Acid-Promoted Formation of Stabilized Silylium Ions for Catalytic Friedel−Crafts C−H Silylation. *J. Am. Chem. Soc.* **2016**, *138*, 7868−7871.
(39) Hua, Y.; Asgari, P.; Avullala, T.; Jeon, J. Catalytic Reductive *ortho*-C−H Silylation of Phenols with Traceless, Versatile Acetal Directing Groups and Synthetic Applications of Dioxasilines. *J. Am. Chem. Soc.* **2016**, *138*, 7982−7991.
(40) Lee, K.-s.; Katsoulis, D.; Choi, J. Intermolecular C−H Silylation of Arenes and Heteroarenes with $HSiEt_3$ under Operationally Diverse Conditions: Neat/Stoichiometric and Acceptor/Acceptorless. *ACS Catal.* **2016**, *6*, 1493−1496.
(41) Li, W.; Huang, X.; You, J. Ruthenium-Catalyzed Intermolecular Direct Silylation of Unreactive C(sp^3)−H Bonds. *Org. Lett.* **2016**, *18*, 666−668.
(42) Fang, H.; Hou, W.; Liu, G.; Huang, Z. Ruthenium-Catalyzed Site-Selective Intramolecular Silylation of Primary C−H Bonds for Synthesis of Sila-Heterocycles. *J. Am. Chem. Soc.* **2017**, *139*, 11601−11609.
(43) Xu, Z.; Chai, L.; Liu, Z.-Q. Free-Radical-Promoted Site-Selective C−H Silylation of Arenes by Using Hydrosilanes. *Org. Lett.* **2017**, *19*, 5573−5576.
(44) Yonekura, K.; Iketani, Y.; Sekine, M.; Tani, T.; Matsui, F.; Kamakura, D.; Tsuchimoto, T. Zinc-Catalyzed Dehydrogenative Silylation of Indoles. *Organometallics* **2017**, *36*, 3234−3249.
(45) Rubio-Pérez, L.; Iglesias, M.; Munárriz, J.; Polo, V.; Passarelli, V.; Pérez-Torrente, J. J.; Oro, L. A. A Well-Defined NHC−Ir(III) Catalyst for the Silylation of Aromatic C−H Bonds: Substrate Survey and Mechanistic Insights. *Chem. Sci.* **2017**, *8*, 4811−4822.

https://dx.doi.org/10.1021/jacs.0c13335
J. Am. Chem. Soc. 2021, 143, 3571−3582

(46) Fukumoto, Y.; Hirano, M.; Chatani, N. Iridium-Catalyzed Regioselective C(sp^3)−H Silylation of 4-Alkylpyridines at the Benzylic Position with Hydrosilanes Leading to 4-(1-Silylalkyl)-pyridines. *ACS Catal.* **2017**, *7*, 3152−3156.
(47) Luo, Y.; Teng, H.-L.; Xue, C.; Nishiura, M.; Hou, Z. Yttrium-Catalyzed Regioselective α-C−H Silylation of Methyl Sulfides with Hydrosilanes. *ACS Catal.* **2018**, *8*, 8027−8032.
(48) Bunescu, A.; Butcher, T. W.; Hartwig, J. F. Traceless Silylation of β-C(sp^3)−H Bonds of Alcohols via Perfluorinated Acetals. *J. Am. Chem. Soc.* **2018**, *140*, 1502−1507.
(49) Xu, W.; Teng, H.; Luo, Y.; Lou, S.; Nishiura, M.; Hou, Z. Rare-Earth-Catalyzed C−H Silylation of Aromatic Heterocycles with Hydrosilanes. *Chem. - Asian J.* **2020**, *15*, 753−756.
(50) Mu, D.; Yuan, W.; Chen, S.; Wang, N.; Yang, B.; You, L.; Zu, B.; Yu, P.; He, C. Streamlined Construction of Silicon-Stereogenic Silanes by Tandem Enantioselective C−H Silylation/Alkene Hydrosilylation. *J. Am. Chem. Soc.* **2020**, *142*, 13459−13468.
(51) Yang, B.; Yang, W.; Guo, Y.; You, L.; He, C. Enantioselective Silylation of Aliphatic C−H Bonds for the Synthesis of Silicon-Stereogenic Dihydrobenzosiloles. *Angew. Chem., Int. Ed.* **2020**, *59*, 22217−22222.
(52) Yuan, W.; You, L.; Lin, W.; Ke, J.; Li, Y.; He, C. Asymmetric Synthesis of Silicon-Stereogenic Monohydrosilanes by Dehydrogenative C−H Silylation. *Org. Lett.* **2021**, DOI: 10.1021/acs.orglett.1c00029.
(53) Ishikawa, M.; Okazaki, S.; Naka, A.; Sakamoto, H. Nickel-Catalyzed Reactions of 3,4-Benzo-1,1,2,2-tetraethyl-1,2-disilacyclobutene with Aromatic Compounds. *Organometallics* **1992**, *11*, 4135−4139.
(54) Ishiyama, T.; Sato, K.; Nishio, Y.; Saiki, T.; Miyaura, N. Regioselective Aromatic C−H Silylation of Five-Membered Heteroarenes with Fluorodisilanes Catalyzed by Iridium(I) Complexes. *Chem. Commun.* **2005**, 5065−5067.
(55) Chen, C.; Guan, M.; Zhang, J.; Wen, Z.; Zhao, Y. Palladium-Catalyzed Oxalyl Amide Directed Silylation and Germanylation of Amine Derivatives. *Org. Lett.* **2015**, *17*, 3646−3649.
(56) Liu, Y.-J.; Liu, Y.-H.; Zhang, Z.-Z.; Yan, S.-Y.; Chen, K.; Shi, B.-F. Divergent and Stereoselective Synthesis of β-Silyl-α-Amino Acids through Palladium-Catalyzed Intermolecular Silylation of Unactivated Primary and Secondary C−H Bonds. *Angew. Chem., Int. Ed.* **2016**, *55*, 13859−13862.
(57) Pan, J.-L.; Li, Q.-Z.; Zhang, T.-Y.; Hou, S.-H.; Kang, J.-C.; Zhang, S.-Y. Palladium-Catalyzed Direct Intermolecular Silylation of Remote Unactivated C(sp^3)−H Bonds. *Chem. Commun.* **2016**, *52*, 13151−13154.
(58) Modak, A.; Patra, T.; Chowdhury, R.; Raul, S.; Maiti, D. Palladium-Catalyzed Remote *meta*-Selective C−H Bond Silylation and Germanylation. *Organometallics* **2017**, *36*, 2418−2423.
(59) Oestreich, M.; Hartmann, E.; Mewald, M. Activation of the Si−B Interelement Bond: Mechanism, Catalysis, and Synthesis. *Chem. Rev.* **2013**, *113*, 402−441.
(60) Feng, J.-J.; Mao, W.; Zhang, L.; Oestreich, M. Activation of the Si−B Interelement Bond Related to Catalysis. *Chem. Soc. Rev.* **2021**, *50*, 2010−2073.
(61) Matsuda, T.; Kadowaki, S.; Yamaguchi, Y.; Murakami, M. Gold-Catalysed Intramolecular *trans*-Allylsilylation of Alkynes Forming 3-Allyl-1-silaindenes. *Chem. Commun.* **2008**, *24*, 2744−2746.
(62) Tobisu, M.; Onoe, M.; Kita, Y.; Chatani, N. Rhodium-Catalyzed Coupling of 2-Silylphenylboronic Acids with Alkynes Leading to Benzosiloles: Catalytic Cleavage of the Carbon−Silicon Bond in Trialkylsilyl Groups. *J. Am. Chem. Soc.* **2009**, *131*, 7506−7507.
(63) Liang, Y.; Zhang, S.; Xi, Z. Palladium-Catalyzed Synthesis of Benzosilolo[2,3-*b*]indoles via Cleavage of a C(sp^3)−Si Bond and Consequent Intramolecular C(sp^2)−Si Coupling. *J. Am. Chem. Soc.* **2011**, *133*, 9204−9207.
(64) Liang, Y.; Geng, W.; Wei, J.; Xi, Z. Palladium-Catalyzed Intermolecular Coupling of 2-Silylaryl Bromides with Alkynes: Synthesis of Benzosiloles and Heteroarene-Fused Siloles by Catalytic Cleavage of the C(sp^3)−Si Bond. *Angew. Chem., Int. Ed.* **2012**, *51*, 1934−1937.
(65) Onoe, M.; Baba, K.; Kim, Y.; Kita, Y.; Tobisu, M.; Chatani, N. Rhodium-Catalyzed Carbon−Silicon Bond Activation for Synthesis of Benzosilole Derivatives. *J. Am. Chem. Soc.* **2012**, *134*, 19477−19488.
(66) Meng, T.; Ouyang, K.; Xi, Z. Palladium-Catalyzed Cleavage of the Me−Si Bond in *ortho*-Trimethylsilyl Aryltriflates: Synthesis of Benzosilole Derivatives from *ortho*-Trimethylsilyl Aryltriflates and Alkynes. *RSC Adv.* **2013**, *3*, 14273−14276.
(67) Zhang, Q.-W.; An, K.; He, W. Rhodium-Catalyzed Tandem Cyclization/Si−C Activation Reaction for the Synthesis of Siloles. *Angew. Chem., Int. Ed.* **2014**, *53*, 5667−5671.
(68) Elsby, M. R.; Johnson, S. A. Nickel-Catalyzed C−H Silylation of Arenes with Vinylsilanes: Rapid and Reversible β-Si Elimination. *J. Am. Chem. Soc.* **2017**, *139*, 9401−9407.
(69) Godula, K.; Sames, D. C−H Bond Functionalization in Complex Organic Synthesis. *Science* **2006**, *312*, 67−72.
(70) Díaz-Requejo, M. M.; Pérez, P. J. Coinage Metal Catalyzed C−H Bond Functionalization of Hydrocarbons. *Chem. Rev.* **2008**, *108*, 3379−3394.
(71) Yamaguchi, J.; Yamaguchi, A. D.; Itami, K. C−H Bond Functionalization: Emerging Synthetic Tools for Natural Products and Pharmaceuticals. *Angew. Chem., Int. Ed.* **2012**, *51*, 8960−9009.
(72) Zhang, Y.-H.; Shi, G.-F.; Yu, J.-Q. 3.23 Carbon−Carbon σ-Bond Formation via C−H Bond Functionalization. In *Comprehensive Organic Synthesis II*, 2nd ed.; Elsevier: Amsterdam, 2014; pp 1101−1209.
(73) Dixneuf, P. H.; Doucet, H. *C−H Bond Activation and Catalytic Functionalization I*; Springer: Cham, 2016.
(74) Hartwig, J. F.; Larsen, M. A. Undirected, Homogeneous C−H Bond Functionalization: Challenges and Opportunities. *ACS Cent. Sci.* **2016**, *2*, 281−292.
(75) Gandeepan, P.; Müller, T.; Zell, D.; Cera, G.; Warratz, S.; Ackermann, L. 3d Transition Metals for C−H Activation. *Chem. Rev.* **2019**, *119*, 2192−2452.
(76) Rej, S.; Das, A.; Chatani, N. Strategic Evolution in Transition Metal-Catalyzed Directed C−H Bond Activation and Future Directions. *Coord. Chem. Rev.* **2021**, *431*, 213683.
(77) Sommer, L. H.; Baum, G. A. A Silicon-Containing 4-Ring. *J. Am. Chem. Soc.* **1954**, *76*, 5002.
(78) Golino, C. M.; Bush, R. D.; Sommer, L. H. Silicon-Carbon Multiple-Bonded (p_π−p_π) Intermediates. First Generation and Reactions of Silaethene [$H_2Si = CH_2$] and Silanone [$H_2Si = O$]. *J. Am. Chem. Soc.* **1975**, *97*, 7371−7372.
(79) Myers, A. G.; Kephart, S. E.; Chen, H. Silicon-Directed Aldol Reactions. Rate Acceleration by Small Rings. *J. Am. Chem. Soc.* **1992**, *114*, 7922−7923.
(80) Matsumoto, K.; Oshima, K.; Utimoto, K. Noncatalyzed Stereoselective Allylation of Carbonyl Compounds with Allylsilacyclobutanes. *J. Org. Chem.* **1994**, *59*, 7152−7155.
(81) For a review, see: Denmark, S. E.; Sweis, R. F. Design and Implementation of New, Silicon-Based, Cross-Coupling Reactions: Importance of Silicon−Oxygen Bonds. *Acc. Chem. Res.* **2002**, *35*, 835−846.
(82) Hirano, K.; Yorimitsu, H.; Oshima, K. Nickel-Catalyzed Regio- and Stereoselective Silylation of Terminal Alkenes with Silacyclobutanes: Facile Access to Vinylsilanes from Alkenes. *J. Am. Chem. Soc.* **2007**, *129*, 6094−6095.
(83) Shintani, R.; Moriya, K.; Hayashi, T. Palladium-Catalyzed Enantioselective Desymmetrization of Silacyclobutanes: Construction of Silacycles Possessing a Tetraorganosilicon Stereocenter. *J. Am. Chem. Soc.* **2011**, *133*, 16440−16443.
(84) Shintani, R.; Moriya, K.; Hayashi, T. Palladium-Catalyzed Desymmetrization of Silacyclobutanes with Alkynes: Enantioselective Synthesis of Silicon-Stereogenic 1-Sila-2-cyclohexenes and Mechanistic Considerations. *Org. Lett.* **2012**, *14*, 2902−2905.
(85) Chen, H.; Chen, Y.; Tang, X.; Liu, S.; Wang, R.; Hu, T.; Gao, L.; Song, Z. Rhodium-Catalyzed Reaction of Silacyclobutanes with

Unactivated Alkynes to Afford Silacyclohexenes. *Angew. Chem., Int. Ed.* **2019**, *58*, 4695−4699.
(86) Wang, X.-B.; Zheng, Z.-J.; Xie, J.-L.; Gu, W.-X.; Mu, Q.-C.; Yin, G.-W.; Ye, F.; Xu, Z.; Xu, L.-W. Controllable Si−C Bond Activation Enables Stereocontrol in Palladium-Catalyzed [4 + 2] Annulation of Cyclopropenes with Benzosilacyclobutanes. *Angew. Chem., Int. Ed.* **2020**, *59*, 790−797.
(87) Saito, S.; Yoshizawa, T.; Ishigami, S.; Yamasaki, R. Ring Expansion Reactions of Ethyl Cyclopropylideneacetate and Benzosilacyclobutenes: Formal σ Bond Cross Metathesis. *Tetrahedron Lett.* **2010**, *51*, 6028−6030.
(88) Ishida, N.; Ikemoto, W.; Murakami, M. Cleavage of C−C and C−Si σ-Bonds and Their Intramolecular Exchange. *J. Am. Chem. Soc.* **2014**, *136*, 5912−5915.
(89) Okumura, S.; Sun, F.; Ishida, N.; Murakami, M. Palladium-Catalyzed Intermolecular Exchange between C−C and C−Si σ-Bonds. *J. Am. Chem. Soc.* **2017**, *139*, 12414−12417.
(90) Zhao, W.-T.; Gao, F.; Zhao, D. Intermolecular σ-Bond Cross-Exchange Reaction between Cyclopropenones and (Benzo)-silacyclobutanes: Straightforward Access towards Sila(benzo)-cycloheptenones. *Angew. Chem., Int. Ed.* **2018**, *57*, 6329−6332.
(91) For a metal-free formal [4 + 2] cycloaddition of SCBs with CO_2, see: Ishida, N.; Okumura, S.; Kawasaki, T.; Murakami, M. 2-Arylsilacyclobutane as a Latent Carbanion Reacting with CO_2. *Angew. Chem., Int. Ed.* **2018**, *57*, 11399−11403.
(92) For a related ring expansion reaction, see: Qin, Y.; Han, J.-L.; Ju, C.-W.; Zhao, D. Ring Expansion to 6-, 7-, and 8-Membered Benzosilacycles through Strain-Release Silicon-Based Cross-Coupling. *Angew. Chem., Int. Ed.* **2020**, *59*, 8481−8485.
(93) Zhang, Q.-W.; An, K.; Liu, L.-C.; Guo, S.; Jiang, C.; Guo, H.; He, W. Rhodium-Catalyzed Intramolecular C−H Silylation by Silacyclobutanes. *Angew. Chem., Int. Ed.* **2016**, *55*, 6319−6323.
(94) Zhang, Q.-W.; An, K.; Liu, L.-C.; Zhang, Q.; Guo, H.; He, W. Construction of Chiral Tetraorganosilicons by Tandem Desymmetrization of Silacyclobutanes/Intermolecular Dehydrogenative Silylation. *Angew. Chem., Int. Ed.* **2017**, *56*, 1125−1129.
(95) Cheng, C.; Hartwig, J. F. Mechanism of the Rhodium-Catalyzed Silylation of Arene C−H Bonds. *J. Am. Chem. Soc.* **2014**, *136*, 12064−12072.
(96) Lee, T.; Hartwig, J. F. Mechanistic Studies on Rhodium-Catalyzed Enantioselective Silylation of Aryl C−H Bonds. *J. Am. Chem. Soc.* **2017**, *139*, 4879−4886.
(97) Liu, W.-B.; Schuman, D. P.; Yang, Y.-F.; Toutov, A. A.; Liang, Y.; Klare, H. F. T.; Nesnas, N.; Oestreich, M.; Blackmond, D. G.; Virgil, S. C.; Banerjee, S.; Zare, R. N.; Grubbs, R. H.; Houk, K. N.; Stoltz, B. M. Potassium *tert*-Butoxide-Catalyzed Dehydrogenative C−H Silylation of Heteroaromatics: A Combined Experimental and Computational Mechanistic Study. *J. Am. Chem. Soc.* **2017**, *139*, 6867−6879.
(98) Banerjee, S.; Yang, Y.-F.; Jenkins, I. D.; Liang, Y.; Toutov, A. A.; Liu, W.-B.; Schuman, D. P.; Grubbs, R. H.; Stoltz, B. M.; Krenske, E. H.; Houk, K. N.; Zare, R. N. Ionic and Neutral Mechanisms for C−H Bond Silylation of Aromatic Heterocycles Catalyzed by Potassium *tert*-Butoxide. *J. Am. Chem. Soc.* **2017**, *139*, 6880−6887.
(99) Murai, M.; Okada, R.; Asako, S.; Takai, K. Rhodium-Catalyzed Silylative and Germylative Cyclization with Dehydrogenation Leading to 9-Sila- and 9-Germafluorenes: A Combined Experimental and Computational Mechanistic Study. *Chem. - Eur. J.* **2017**, *23*, 10861−10870.
(100) Karmel, C.; Li, B.; Hartwig, J. F. Rhodium-Catalyzed Regioselective Silylation of Alkyl C−H Bonds for the Synthesis of 1,4-Diols. *J. Am. Chem. Soc.* **2018**, *140*, 1460−1470.
(101) Karmel, C.; Hartwig, J. F. Mechanism of the Iridium-Catalyzed Silylation of Aromatic C−H Bonds. *J. Am. Chem. Soc.* **2020**, *142*, 10494−10505.
(102) Esteruelas, M. A.; Martínez, A.; Oliván, M.; Oñate, E. Kinetic Analysis and Sequencing of Si−H and C−H Bond Activation Reactions: Direct Silylation of Arenes Catalyzed by an Iridium-Polyhydride. *J. Am. Chem. Soc.* **2020**, *142*, 19119−19131.
(103) Zhang, J.; Xu, J.-Z.; Zheng, Z.-J.; Xu, Z.; Cui, Y.-M.; Cao, J.; Xu, L.-W. Palladium-Catalyzed Desymmetrization of Silacyclobutanes with Alkynes to Silicon-Stereogenic Silanes: A Density Functional Theory Study. *Chem. - Asian J.* **2016**, *11*, 2867−2875.
(104) Xu, Z.-Y.; Zhang, S.-Q.; Liu, J.-R.; Chen, P.-P.; Li, X.; Yu, H.-Z.; Hong, X.; Fu, Y. Mechanism and Origins of Chemo- and Regioselectivities of Pd-Catalyzed Intermolecular σ-Bond Exchange between Benzocyclobutenones and Silacyclobutanes: A Computational Study. *Organometallics* **2018**, *37*, 592−602.
(105) Liu, S.; Zhang, T.; Zhu, L.; Liu, F.; Bai, R.; Lan, Y. Layered Chirality Relay Model in Rh(I)-Mediated Enantioselective C−Si Bond Activation: A Theoretical Study. *Org. Lett.* **2020**, *22*, 2124−2128.
(106) McDermott, J. X.; White, J. F.; Whitesides, G. M. Preparation and Thermal Decomposition of Platinum(II) Metallocycles. *J. Am. Chem. Soc.* **1973**, *95*, 4451−4452.
(107) McDermott, J. X.; White, J. F.; Whitesides, G. M. Thermal Decomposition of Bis(phosphine)platinum(II) Metallocycles. *J. Am. Chem. Soc.* **1976**, *98*, 6521−6528.
(108) Gridnev, I. D.; Kouchi, M.; Sorimachi, K.; Terada, M. On the Mechanism of Stereoselection in Direct Mannich Reaction Catalyzed by BINOL-Derived Phosphoric Acids. *Tetrahedron Lett.* **2007**, *48*, 497−500.
(109) Marcelli, T.; Hammar, P.; Himo, F. Phosphoric Acid Catalyzed Enantioselective Transfer Hydrogenation of Imines: A Density Functional Theory Study of Reaction Mechanism and the Origins of Enantioselectivity. *Chem. - Eur. J.* **2008**, *14*, 8562−8571.
(110) Lu, G.; Liu, R. Y.; Yang, Y.; Fang, C.; Lambrecht, D. S.; Buchwald, S. L.; Liu, P. Ligand−Substrate Dispersion Facilitates the Copper-Catalyzed Hydroamination of Unactivated Olefins. *J. Am. Chem. Soc.* **2017**, *139*, 16548−16555.
(111) Xi, Y.; Su, B.; Qi, X.; Pedram, S.; Liu, P.; Hartwig, J. F. Application of Trimethylgermanyl-Substituted Bisphosphine Ligands with Enhanced Dispersion Interactions to Copper-Catalyzed Hydroboration of Disubstituted Alkenes. *J. Am. Chem. Soc.* **2020**, *142*, 18213−18222.
(112) Su, P.; Jiang, Z.; Chen, Z.; Wu, W. Energy Decomposition Scheme Based on the Generalized Kohn−Sham Scheme. *J. Phys. Chem. A* **2014**, *118*, 2531−2542.
(113) Su, P.; Tang, Z.; Wu, W. Generalized Kohn−Sham Energy Decomposition Analysis and Its Applications. *Wiley Interdiscip. Rev.: Comput. Mol. Sci.* **2020**, *10*, No. e1460.
(114) Meißner, A.; Preetz, A.; Drexler, H.-J.; Baumann, W.; Spannenberg, A.; König, A.; Heller, D. Situ Synthesis of Neutral Dinuclear Rhodium Diphosphine Complexes [{Rh(diphosphine)(μ_2-X)}$_2$]: Systematic Investigations. *ChemPlusChem* **2015**, *80*, 169−180.
(115) Becke, A. D. Density-Functional Thermochemistry. III. The Role of Exact Exchange. *J. Chem. Phys.* **1993**, *98*, 5648−5652.
(116) Lee, C.; Yang, W.; Parr, R. G. Development of the Colle−Salvetti Correlation-Energy Formula into a Functional of the Electron Density. *Phys. Rev. B: Condens. Matter Mater. Phys.* **1988**, *37*, 785−789.
(117) Frisch, M. J.; Trucks, G. W.; Schlegel, H. B.; Scuseria, G. E.; Robb, M. A.; Cheeseman, J. R.; Scalmani, G.; Barone, V.; Mennucci, B.; Petersson, G. A.; Nakatsuji, H.; Caricato, M.; Li, X.; Hratchian, H. P.; Izmaylov, A. F.; Bloino, J.; Zheng, G.; Sonnenberg, J. L.; Hada, M.; Ehara, M.; Toyota, K.; Fukuda, R.; Hasegawa, J.; Ishida, M.; Nakajima, T.; Honda, Y.; Kitao, O.; Nakai, H.; Vreven, T.; Montgomery, J. A., Jr.; Peralta, J. E.; Ogliaro, F.; Bearpark, M.; Heyd, J. J.; Brothers, E.; Kudin, K. N.; Staroverov, V. N.; Kobayashi, R.; Normand, J.; Raghavachari, K.; Rendell, A.; Burant, J. C.; Iyengar, S. S.; Tomasi, J.; Cossi, M.; Rega, N.; Millam, M. J.; Klene, M.; Knox, J. E.; Cross, J. B.; Bakken, V.; Adamo, C.; Jaramillo, J.; Gomperts, R.; Stratmann, R. E.; Yazyev, O.; Austin, A. J.; Cammi, R.; Pomelli, C.; Ochterski, J. W.; Martin, R. L.; Morokuma, K.; Zakrzewski, V. G.; Voth, G. A.; Salvador, P.; Dannenberg, J. J.; Dapprich, S.; Daniels, A. D.; Farkas, Ö.; Foresman, J. B.; Ortiz, J. V.; Cioslowski, J.; Fox, D. J. *Gaussian 09*, Revision D.01; Gaussian, Inc.: Wallingford, CT, 2013.

https://dx.doi.org/10.1021/jacs.0c13335
J. Am. Chem. Soc. 2021, 143, 3571−3582

(118) Hehre, W. J.; Radom, L.; Schleyer, P. v. R.; Pople, J. A. *Ab Initio Molecular Orbital Theory*; Wiley: New York, 1986.
(119) Hay, P. J.; Wadt, W. R. Ab Initio Effective Core Potentials for Molecular Calculations. Potentials for K to Au Including the Outermost Core Orbitals. *J. Chem. Phys.* **1985**, *82*, 299−310.
(120) Marenich, A. V.; Cramer, C. J.; Truhlar, D. G. Universal Solvation Model Based on Solute Electron Density and on a Continuum Model of the Solvent Defined by the Bulk Dielectric Constant and Atomic Surface Tensions. *J. Phys. Chem. B* **2009**, *113*, 6378−6396.
(121) Grimme, S.; Antony, J.; Ehrlich, S.; Krieg, H. A Consistent and Accurate Ab Initio Parametrization of Density Functional Dispersion Correction (DFT-D) for the 94 Elements H−Pu. *J. Chem. Phys.* **2010**, *132*, 154104.
(122) Grimme, S.; Ehrlich, S.; Goerigk, L. Effect of the Damping Function in Dispersion Corrected Density Functional Theory. *J. Comput. Chem.* **2011**, *32*, 1456−1465.
(123) Weigend, F.; Ahlrichs, R. Balanced Basis Sets of Split Valence, Triple Zeta Valence and Quadruple Zeta Valence Quality for H to Rn: Design and Assessment of Accuracy. *Phys. Chem. Chem. Phys.* **2005**, *7*, 3297−3305.
(124) Andrae, D.; Häußermann, U.; Dolg, M.; Stoll, H.; Preuß, H. Energy-Adjusted Ab Initio Pseudopotentials for the Second and Third Row Transition Elements. *Theor. Chim. Acta* **1990**, *77*, 123−141.
(125) Schmidt, M. W.; Baldridge, K. K.; Boatz, J. A.; Elbert, S. T.; Gordon, M. S.; Jensen, J. H.; Koseki, S.; Matsunaga, N.; Nguyen, K. A.; Su, S.; Windus, T. L.; Dupuis, M.; Montgomery, J. A., Jr. General Atomic and Molecular Electronic Structure System. *J. Comput. Chem.* **1993**, *14*, 1347−1363.
(126) Legault, C. Y. CYLview, 1.0b; Université de Sherbrooke: Quebec, Canada, 2009; http://www.cylview.org.
(127) Poater, A.; Ragone, F.; Mariz, R.; Dorta, R.; Cavallo, L. Comparing the Enantioselective Power of Steric and Electrostatic Effects in Transition-Metal-Catalyzed Asymmetric Synthesis. *Chem. - Eur. J.* **2010**, *16*, 14348−14353.
(128) Falivene, L.; Credendino, R.; Poater, A.; Petta, A.; Serra, L.; Oliva, R.; Scarano, V.; Cavallo, L. SambVca 2. A Web Tool for Analyzing Catalytic Pockets with Topographic Steric Maps. *Organometallics* **2016**, *35*, 2286−2293.
(129) Falivene, L.; Cao, Z.; Petta, A.; Serra, L.; Poater, A.; Oliva, R.; Scarano, V.; Cavallo, L. Towards the Online Computer-Aided Design of Catalytic Pockets. *Nat. Chem.* **2019**, *11*, 872−879.
(130) Park, S. H.; Kwak, J.; Shin, K.; Ryu, J.; Park, Y.; Chang, S. Mechanistic Studies of the Rhodium-Catalyzed Direct C−H Amination Reaction Using Azides as the Nitrogen Source. *J. Am. Chem. Soc.* **2014**, *136*, 2492−2502.
(131) Wang, K.; Chen, P.; Ji, D.; Zhang, X.; Xu, G.; Sun, J. Rhodium-Catalyzed Regioselective N^2-Alkylation of Benzotriazoles with Diazo Compounds/Enynones via a Nonclassical Pathway. *Angew. Chem., Int. Ed.* **2018**, *57*, 12489−12493.
(132) Meng, X.; Yang, B.; Zhang, L.; Pan, G.; Zhang, X.; Shao, Z. Rh(II)/Brønsted Acid Catalyzed General and Highly Diastereo- and Enantioselective Propargylation of *in Situ* Generated Oxonium Ylides and *C*-Alkynyl *N*-Boc *N*,*O*-Acetals: Synthesis of Polyfunctional Propargylamines. *Org. Lett.* **2019**, *21*, 1292−1296.
(133) Chen, L.; Zhang, L.; Shao, Y.; Xu, G.; Zhang, X.; Tang, S.; Sun, J. Rhodium-Catalyzed C = N Bond Formation through a Rebound Hydrolysis Mechanism and Application in *β*-Lactam Synthesis. *Org. Lett.* **2019**, *21*, 4124−4127.
(134) Adamo, C.; Barone, V. Toward Reliable Density Functional Methods without Adjustable Parameters: The PBE0 Model. *J. Chem. Phys.* **1999**, *110*, 6158−6170.
(135) Zhao, Y.; Truhlar, D. The M06 Suite of Density Functionals for Main Group Thermochemistry, Thermochemical Kinetics, Noncovalent Interactions, Excited States, and Transition Elements: Two New Functionals and Systematic Testing of Four M06-Class Functionals and 12 Other Functionals. *Theor. Chem. Acc.* **2008**, *120*, 215−241.
(136) Chai, J.-D.; Head-Gordon, M. Long-Range Corrected Hybrid Density Functionals with Damped Atom−Atom Dispersion Corrections. *Phys. Chem. Chem. Phys.* **2008**, *10*, 6615−6620.

https://dx.doi.org/10.1021/jacs.0c13335
J. Am. Chem. Soc. 2021, 143, 3571−3582